Dynamics of Solar Magnetic Fields
A Spectroscopic Investigation

Michael Sigwarth

National Solar Observatory/Sacramento Peak
Sunspot, NM 88349, USA
sigwarth@sunspot.noao.edu

Abstract

The development of high precision polarimeter and the widened capability of existing solar telescopes for high resolution observations during the last decade opened the possibility to investigate the flows within small scale magnetic flux concentration in the solar photosphere. Within magnetic elements, the smallest magnetic flux concentrations in the photosphere with kG field strength, strong up and downflows are present which cannot be observed at low spatial and temporal resolution. The dominance of down streams within magnetic elements are consistent with existing MHD models of flux tubes embedded in the photosphere which interact strongly with convective motions. The temporal evolution of magnetic elements indicate that the formation of flux tubes is correlated with accelerated downflows in the magnetized plasma. This is in accordance to a formation of kG flux tubes by convective collapse, a theoretically predicted instability of flux concentrations with equipartition field strength.

From the dynamical properties of new magnetic flux emerging into the photosphere and forming a bipolar active region, strong indications are found that active regions are formed from flux tubes rising buoyantly from deeper layers into the photosphere.

The results indicate that for a detailed understanding of flux tube dynamics observations beyond the existing diffraction and photon flux limited capabilities of existing solar facilities are necessary.

1 Introduction

Stellar activity like hot and extended coronae, chromospheric activity and starspots are driven by magnetic fields. To understand the generation of the magnetic field and how the activity develops it is necessary to investigate the interaction of magnetic fields and gas motions in the convective stellar envelope (magneto-convection). Only the sun allows observation of photospheric

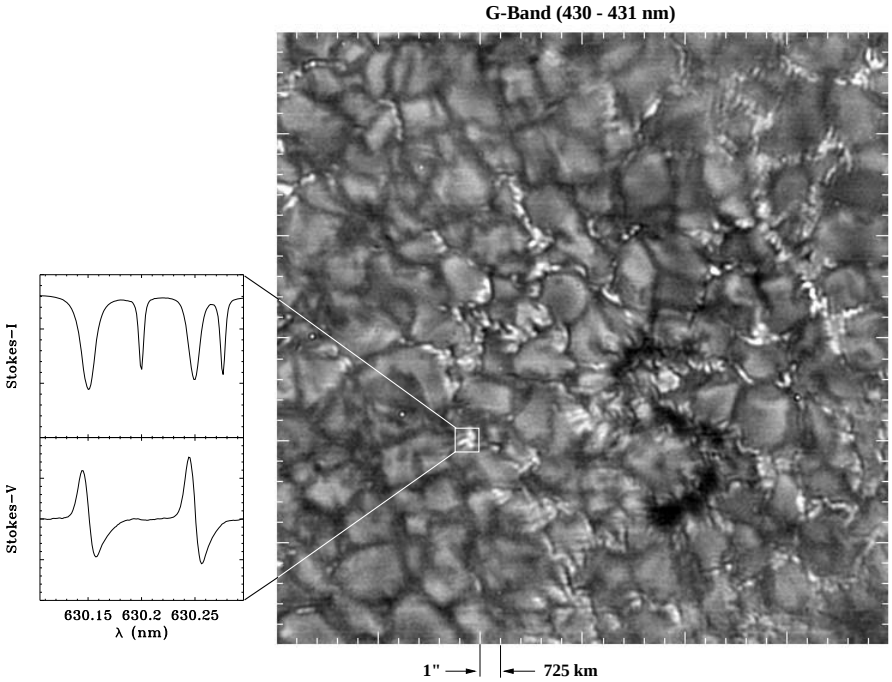

Figure 1: High resolution imaging and high resolution spectroscopy. The image show a 1 nm broad filtergram of an active region taken in the G-band at 430.5 nm (T. Rimmele, NSO). The spatial resolution is close to the diffraction limited resolution of the Dunn Solar Telescope NSO/SP of 0.14 arcsec (100 km) at 430 nm. Due to the longer integration time which is necessary in spectropolarimetric observations with high spectral dispersion, the spatial resolution which can be achieved without real time correction of atmospheric wavefront distortion (adaptive optics) is about 1 arcsec^2, indicated by the white box.

magnetic fields on various scales and with high precision and is therefore the only object to prove directly theoretical models on the formation and transformation of stellar magnetic fields.

The solar magnetic field occurs at the photosphere in flux concentrations of different size and field strength. Sunspots, the most prominent magnetic features, are thought to be built by flux tubes (or bundles of flux tubes), rising buoyantly from the bottom of the convection zone, where the magnetic field is most probably generated by a dynamo (Weiss 1994, Schüssler 1996, Zwaan 1992). By measuring the properties of sunspots, e. g. the tilt of bipolar sunspot groups with respect to the equator or gas flows within and around flux tubes emerging into the photosphere, numerical simulations on rising flux tubes can be proved. In Section 4 of this paper we present observations which strongly support the idea of rising flux tubes leading to bipolar active regions.

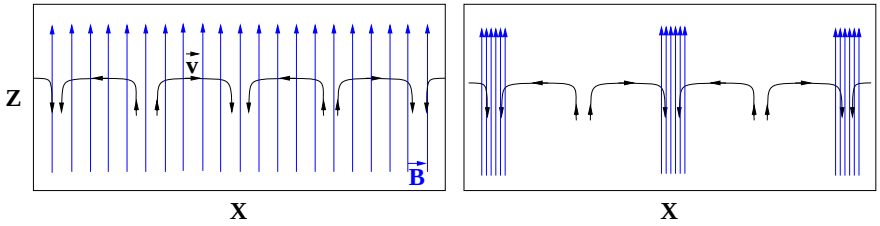

Figure 2: Concentration of magnetic field by flux expulsion. The vertical arrows illustrate the magnetic field lines ($\vec{B}$) which are driven by horizontal convective motions ($\vec{v}$) towards the edge of convective cells (granulation or supergranulation).

The field strength in sunspots reaches up to 0.4 T. But also outside of sunspots about 90 % of the magnetic flux appears as strong fields with field strength of about 0.15 T (Howard & Stenflo 1972, Frazier & Stenflo 1972). These non-spot strong fields mainly appear in plages and at the border of supergranular cells, where they form the magnetic network. High resolution observations (Keller 1992, Berger & Titel 1996) brought direct evidence that these large scale structures are built up from clusters of small, individual magnetic features, called magnetic elements. Figure 1 shows a high resolution image of an active region taken at 430.5 nm where magnetic elements show up as bright points or bright *crincels* mainly located in the intergranular lanes or at the edge of granules. These magnetic elements have field strength between 0.1 and 0.2 T (Stenflo 1973) and sizes from several 100 km down to the diffraction limited resolution of actual solar telescopes of about 150 km. Magnetic elements are described by thin, almost vertical magnetic flux tubes (or clusters of flux tubes) embedded in the intergranular downdraft regions in the photosphere (for review see e. g. Solanki 1993). Mainly inside the network cells, a weaker magnetic component with field strength around 50 mT is present (Lin 1995). There are also hints for a very weak, may be turbulent, background field (Stenflo et al. 1998).

The equipartition field strength, i. e. the equilibrium between the kinetic and magnetic energy density, in the solar photosphere is on granular scales about 50 mT (Galloway & Weiss 1981) which compares well with the field strength of the weak component but is much less then the field strength of magnetic elements and active regions. Therefore there must be an efficient mechanism to increase the field strength to the observed values.

The formation of magnetic elements, but also the interaction of evolved small scale flux tubes with convective motions in the photosphere, should lead to a strongly dynamic behavior of these magnetic features as seen from recent numerical MHD simulations (Steiner et al. 1998, Grossmann-Doerth et al. 1998). Due to such interaction kinetic energy could be transformed into magnetic energy and transported to the chromosphere and transition region along the magnetic field lines.

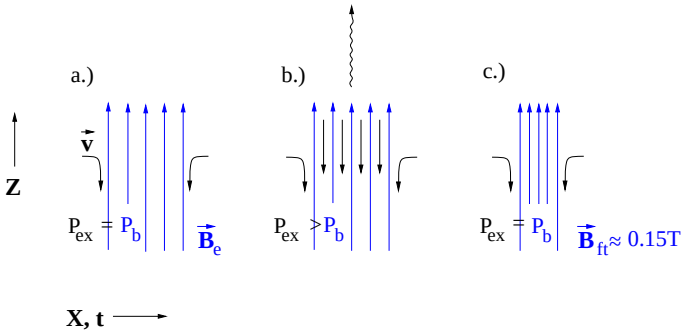

Figure 3: Formation of flux tubes by convective collapse.

Due to the small time and spatial scales on which these effects should take place (typical a few seconds to minutes and below 1 arcsec), it is a challenge for spectroscopic observations to reach these scales.

1.1 Formation of small scale flux tubes

The formation of kG flux tubes is described as a two step process. In a first step magnetic flux is expulsed by horizontal, convective motions towards the granulation and supergranulation boundary (flux expulsion, Parker 1963, Weiss 1966, Galloway & Weiss 1981). Figure 2 illustrate this process in a simplified 2 dimensional representation. For example a homogeneous or turbulent distributed weak magnetic field is *frozen* in the electric conductive plasma and is therefore, driven by convective flows, concentrated in the intergranular lanes and at the supergranular boundaries. Recent large scale numerical MHD simulations show that a substantial fraction of the weak magnetic field can also be generated locally by dynamo action associated with the granular and supergranular flows (Cattaneo 1999). In any case the field strength can only reach up to the equipartition field strength $\vec{B}_e$. This situation is shown in plot a.) of Fig. 3: The flux concentration is located in a downflow environment. There is equilibrium between the external gas pressure P_{ex} and the pressure within the magnetic field P_b which consist of the magnetic pressure ($\sim B^2$) and the internal gas pressure. Because of the increased field strength the horizontal convective gas flows cannot cross the field lines. Therefore a downflow around the flux concentration sets in. Radiative energy losses within the magnetized plasma can no longer be balanced by incoming horizontal gas flows as illustrated in plot b.) of Fig. 3 so that the gas within the magnetic field cools and starts to sink adiabatically in the sub-adiabatic environment which forces the cooling and leads to an accelerated downflow. Due to the downstream the flux tube gets partially evacuated so that now the external gas pressure exceeds the internal pressure and the flux tube starts to concentrate or *collapse* until the increasing magnetic pressure (due to the increasing field strength) bal-

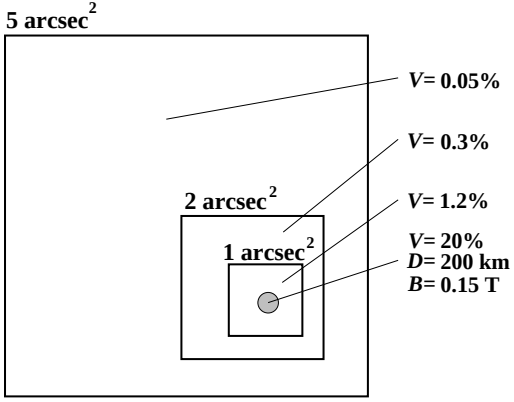

Figure 4: The resulting amplitude of Stokes-V spectra depending on the spatial resolution. Assumed is a flux tube of 200 km diameter with a field strength of 0.15 T. In case of full spatial resolution one would measure a V amplitude of about 20 % (depending on the spectral line). With increasing size of the resolution element the resulting V amplitude decreases.

ances the external pressure again. This process called *convective collapse* was first suggested by Parker (1978) and Spruit & Zweibel (1979) as an efficient mechanism for the formation of typical kG flux tubes. The most prominent signatures of convective collapse therefore should be a rapidly increasing field strength and a strong downflow within the plasma may be followed by an up moving shock. Critical boundary conditions of these models are concerning the mass conservation balance and the stability of flux tubes.

1.2 Spectroscopic investigation of magnetic elements

Information on vertical flows within and around magnetic elements can only be obtained from the Doppler shift of spectral lines. Because of the high dispersion and the limited aperture of actual solar telescopes (0.4–1.5 m), longer integration times are necessary to obtain spectra with sufficient SNR compared to broad-band imaging. Without real-time correction of atmospheric wavefront distortion[1] (seeing) the typical spatial resolution of spectra are in the range of 0.5 arcsec to 2 arcsec (corresponding to 360 km to 1450 km on the sun). Because the size of magnetic elements are smaller, observations in Stokes-I (unpolarized light) integrate over the flux concentration and their surroundings (see also illustration in Fig. 1). The most sensitive tool for the quantitative investigations of small scale magnetic elements is therefore the analysis of circular polarized light, i. e. of Stokes-V spectra. The circular polarized radiation only occurs from the material within the magnetic field, so that even in the case of spatially not resolved magnetic features informations

[1] Adaptive optics for solar application become available for the first time in Sept. 1998 (Rimmele et al. 1999)

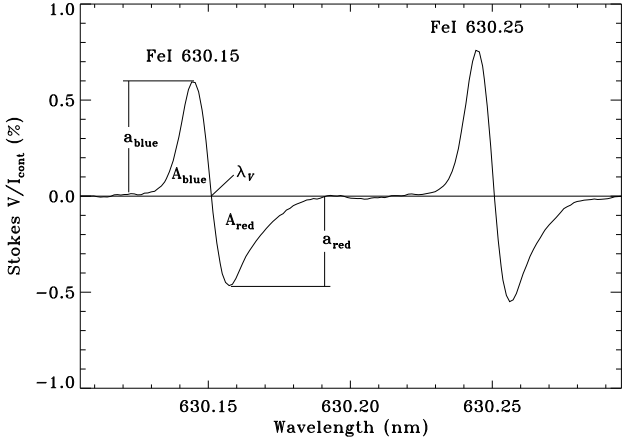

Figure 5: Stokes-V spectra for FeI 630.15 nm ($g_{eff} = 1.67$) and FeI 630.25 nm ($g_{eff} = 2.5$) obtained with the Advanced Stokes Polarimeter in the magnetic network.

on them can be achieved. Critical parameters for the polarimetric observation are polarimetric sensitivity and the fill fraction of the resolution element with magnetic field which depends on the spatial resolution and the size of the magnetic features. Figure 4 illustrate the situation for different spatial resolution. The HAO/NSO Advanced Stokes Polarimeter (ASP, Elmore et al. 1992) which was used for the observations we report here allows measurement of Stokes-V with an RMS continuum noise of $< 3 \cdot 10^{-4}$ of the continuum intensity and to eliminate crosstalk from $I \rightarrow V$ better than $1 \cdot 10^{-3}$. With a spatial resolution of about 1 arcsec^2 this allow to obtain significant V spectra from kG flux tubes down to $\approx$ 150 km diameter. From the Stokes-V spectra the Doppler shift of the zero-crossing point between the blue and red wing of the profile refers to the line-of-sight motion of material within the magnetic field. Figure 5 shows a typical V spectrum obtained in the magnetic network. In a static atmosphere and under the assumption of local thermodynamic equilibrium the Stokes-V profile is expected to be strictly antisymmetric with respect to the zero-crossing wavelength λ_V (Auer & Heasley 1978) and remains unshifted relative to the position of the Stokes-I line core λ_I. Observed V profiles from solar plage and network fields however show a distinct asymmetry between the red and blue wing amplitudes (a_r, a_b) and areas (A_r, A_b) (Stenflo et al. 1984, Wiehr 1985). The asymmetries are expressed in terms of the relative amplitude asymmetry $\delta a = (|a_b| - |a_r|)/(|a_b| + |a_r|)$ and area asymmetry $\delta A = (|A_b| - |A_r|)/(|A_b| + |A_r|)$. At disc center δa and δA are found to be mostly positive with $\delta a > \delta A$ (Solanki & Stenflo 1984, 1985). Towards the limb, δA becomes negative whereas δa is found to stay positive (Stenflo et al. 1987, Martínez Pillet et al. 1997).

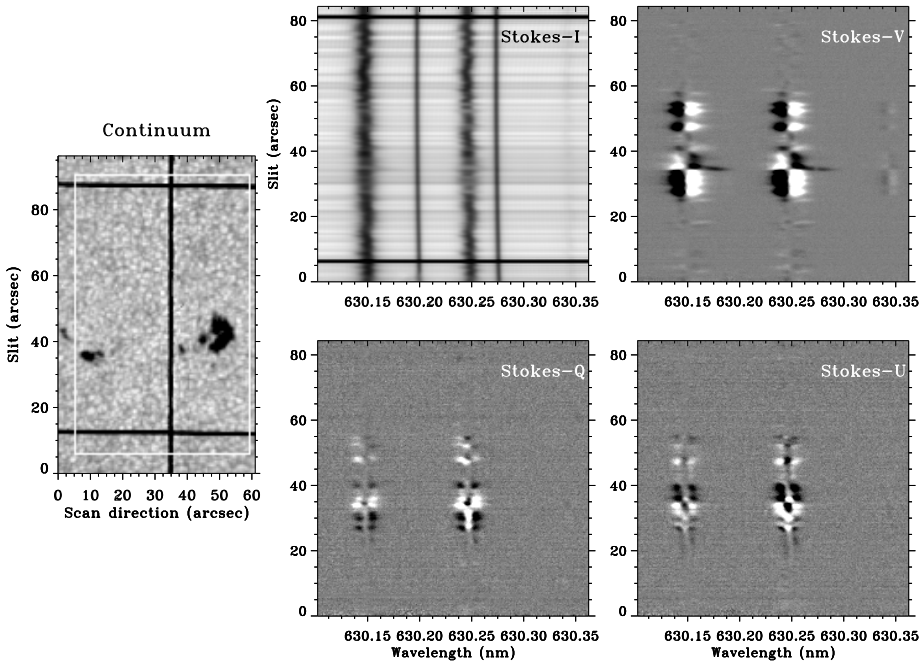

Figure 6: Example for a complete set of high resolution Stokes spectra obtained simultaneously with the ASP. The narrow spectral lines visible in the I spectrum are telluric O_2 lines. The horizontal lines arise from hairlines in front of the entrance slit of the spectrograph. The left image is taken from the reflecting slit jaws. The dark vertical line is the entrance slit. In the horizontal direction the hairlines are visible. By stepping she slit across the field of view a larger area can be scanned. The scanning range for this observation is marked by the white box.

Asymmetric and redshifted V profiles can be reproduced by introducing gradients in downdraft flows and field strength along the formation range of the line (Illing et al. 1974 & 1975, see also Solanki 1993 for review). When observed at low spatial resolution, V profiles behave asymmetrically but do not show a systematic redshift (Stenflo & Harvey 1985, Solanki 1986). Downflows in the non-magnetic surroundings of flux tube while inside no significant flow is present were found to be able to reproduce the observed area asymmetry (Grossmann-Doerth et al. 1988, 1989) without introducing a zero-crossing redshift. In general, interfaces between magnetic and non-magnetic gas with different flows and may be also different temperatures are able to lead to asymmetric profiles (Grossmann-Doerth et al. 1999). Although the mechanisms leading to the V asymmetries are not clearly identified, the dynamic processes in and around the magnetic elements probably play the key role so that the area- and amplitude asymmetry of the V profiles can be used as further parameters to investigate the dynamic behavior of flux tubes.

Since the 1970's, measurements of flows within magnetic elements were performed but no coherent picture could be obtained so far. Early magnetograph measurements (e. g. Giovanelli & Ramsey 1971) leading to downflows between 0.5 and 2 kms^{-1} suffer from low spectral resolution. Due to the asymmetric V profiles, the low spectral resolution can lead to an artificial redshift of the zero crossing λ_V (Solanki & Stenflo 1986). Measurements with the NSO/Kit Peak Fourier Transform Spectrometer (FTS; Brault 1978) have a very high spectral resolution but are spatially and temporally integrated. Due to the absence of absolute wavelength references, λ_V is often measured relative to the mean λ_I position. This leads to uncertainties in determining a possible shift of the V spectra because of the convective blueshifted I profiles (Dravins et al. 1981). Recent investigations of plage fields and quiet sun fields with sensitive vector-polarimeter and a spatial resolution between 1 arcsec and 2 arcsec revealed an increasing downflow within the magnetic field towards smaller fill fraction accompanied by an increase of the scatter of the obtained velocities (Grossmann-Doerth et al. 1996; Martínez Pillet et al. 1997).

1.3 New horizon for solar spectropolarimetry

With the development of sensitive vector-polarimeter like the ASP mentioned above or the Zürich IMaging POLarimeter (ZIMPOL, Povel 1995) it has become possible to perform precise measurements of weak polarization signals. Since the ASP is equipped with a calibration unit, instrumental polarization can be eliminated to a high degree. The operation of the ASP at the Dunn Solar Telescope of the National Solar Observatory further offers the possibility of spatially high resolution observations. Entrance window cooling and the tip tilt correction of image motion (correlation tracker, Rimmele et al. 1991) enhances the achievable spatial resolution of long exposure measurements. Figure 6 shows the example of a typical high resolution dataset obtained with the ASP. The spatial resolution of these spectra is limited by the pixel scale of 0.37×0.6 arcsec^2 per pixel.

2 Statistical investigation of flux tube dynamic

A typical magnetic element in the quiet sun network will not be spatially resolved in spectroscopic measurements. By comparing the intensity of Stokes-I (polarized and unpolarized light) and the total intensity of polarized light (linear and circular) the fill fraction of magnetic field within the resolution element can be estimated (Sigwarth et al. 1999) and therefrom the area covered by magnetic features. A small fill fraction means that probably a single, small-scale flux tube is mapped. But there remains a disambiguity whether the signal really occurs from an individual element or from several small features. On the base of a large number of measurements, weak V signals will originate from only few individual elements with an increasing possibility to catch in-

dividual flux tubes when going to smaller signals. These measurements can then be compared with higher V signals, which originate from larger magnetic features or clusters of flux tubes.

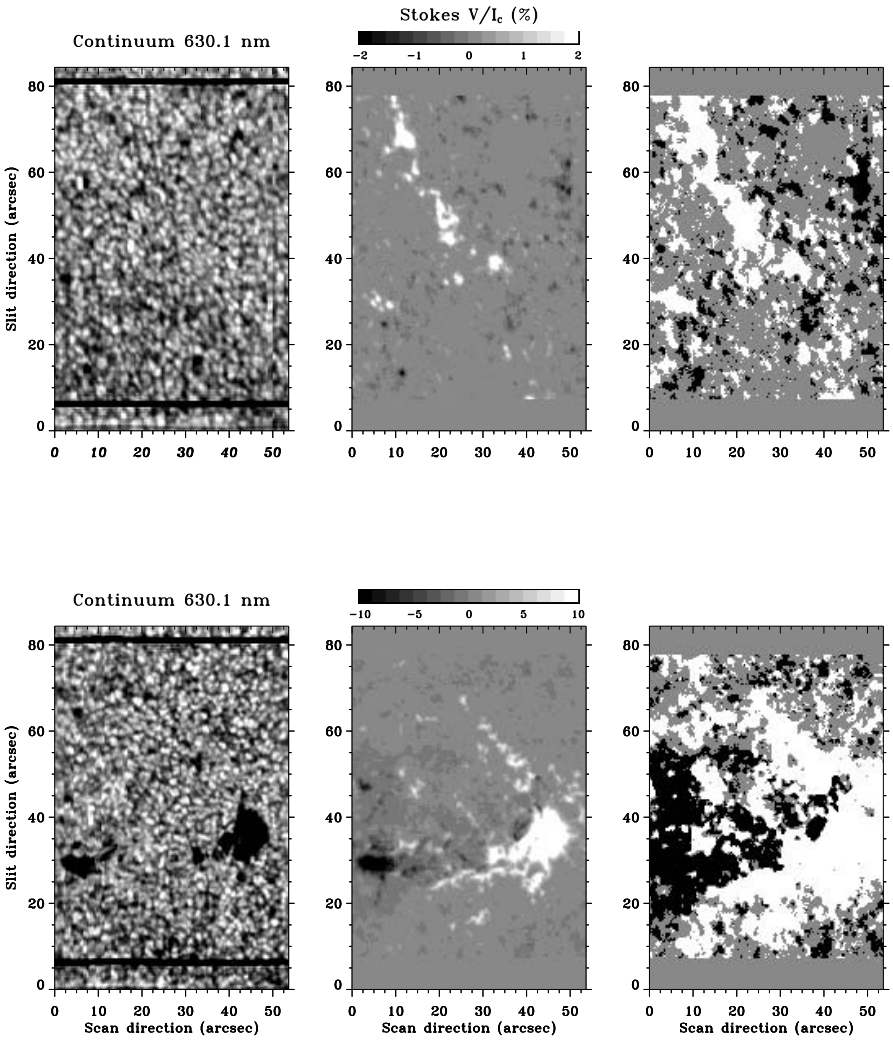

Figure 7: Continuum spectroheliograms and magnetograms from observations of network magnetic fields ("quiet sun"; upper row) and from an active region (bottom row). Each map consist of 144 spectra. In the first row the continuum intensity at 630.1 nm is shown. The second row shows the amplitude of the FeI 630.25 nm V signal. The scaling of the V maps is shown on top. In the right row each data point revealing a V signal $\geq 0.15\,\%$ is shown with respect to the polarity (black-white scaled).

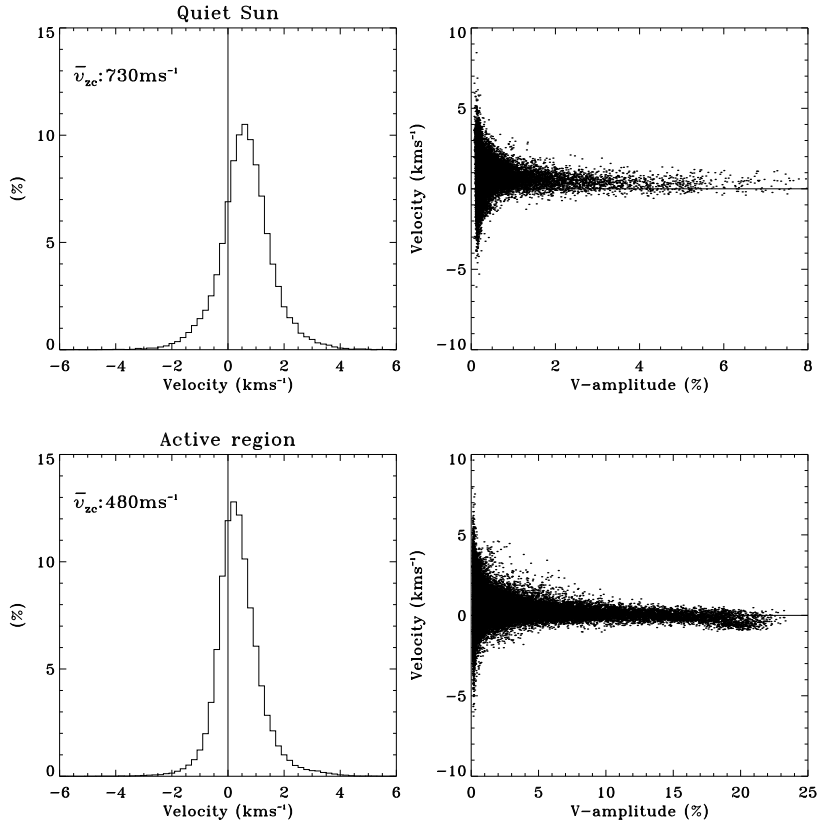

Figure 8: Vertical velocities in magnetic fields obtained from Fe I 630.25 nm Stokes-V. In the right column the distribution of measured velocities in quiet sun magnetic elements (top) and in an active region (bottom) are shown. In the left column the velocities are plotted against the V amplitudes.

By mapping a quiet sun region at disc center and an active region close to disc center 35 000 V profiles from network and internetwork and about 93 000 V profiles from active region plage and sunspots were obtained. The observations where done in June 1996 and July 1997. Figure 7 show examples of spectroheliograms and magnetograms of the 1996 data. Examples for the 1997 observations are shown in Fig. 10. Detailed information on the observation and data reduction are given in Sigwarth et al. (1999a, b) and Sigwarth (1999).

For each V spectra the Doppler shift, i. e. the shift of λ_V, and the area- and amplitude asymmetry were determined. The Doppler shifts were transformed into velocity by means of an absolute velocity calibration using telluric O_2 lines. Excluded from the analysis were V profiles of unusual shape which can originate from different polarities superimposed within the resolution element

	ASP FeI 630.25		ZIMPOL FeI 525	MHD FeI 630.25	FTS FeI 630.25	
	q.s.	a.r.	q.s.	-	Nw	Plage
# Spectra	35000	93000	2228	(1531)*	-	-
v (kms^{-1})	0.73	0.48	0.8	0.74	0.1**	0**
δA (%)	6.1	0.7	3.9	0.4	6	5
δa (%)	14.9	9.4	14.8	14.9	17.8	9.3

Table 1: Mean values of the vertical velocity v within magnetic fields and the area δA and amplitude δa asymmetry of the V profiles of Fe I 630.25 nm in the quiet sun (q. s.) and active region (a. r.). The values are compared with results from ZIMPOL observations (Grossmann-Doerth et al. 1996), from MHD simulations (Steiner 1999) and from FTS observations in the network (Nw) and plage (Solanki & Pahlke 1988). * The calculated V spectra represent different temporal states of a simulated magnetic element. ** The values shown here are corrected for the convective blueshift of Fe I 630.25 nm.

or shocks moving along the flux tube. Profiles with essentially only one wing may represent the extreme case of asymmetric profiles (Sigwarth et al. 1999, Grossmann-Doerth et al. 1999). In total about 10 % of all significant V signals show an unusual shape.

In Fig. 8 the results for the vertical flows within the magnetic fields are shown. On average there remains a downflow > 0.5 kms^{-1} for both, quiet sun and active region fields, but there occurs a substantially different behavior between small and large V amplitude: towards larger V amplitudes the mean velocity decreases. The negative (upward) flows for the strongest signals in the active region occur from the main spot and will be discussed in Sect. 4.

Toward smaller signals, the mean velocity increases. At the same time the scatter of the measured values increase rapidly and exceeds values of 5 kms^{-1} for both up- and downflow. Qualitatively the same is present for the area- and amplitude asymmetry, where on average the asymmetries are positive with exceeding values of 50 % (both positive and negative) towards small V amplitudes. In Tab. 1 the obtained mean values for velocity and profile asymmetry are compared with other measurements and with results from 2D numerical MHD simulations. We were able to measure the influence of noise to these results by comparing the simultaneous measured lines FeI 630.15 nm and Fe I 630.25 nm (see Sigwarth et al. 1999). Down to V amplitudes of 0.5 % noise does not significantly contribute to the measured velocities and amplitude-asymmetries, so that the strong increase in the mean values and the scatter towards smaller V profiles could be proven to be real.

2.1 Discussion and interpretation

How can we interpret the conspicuous change in Doppler shift and asymmetry when going toward smaller V amplitudes? As already mentioned the

possibility to measure a single flux tube increases when going to smaller V amplitudes. Therefore the results indeed show, that small-scale photospheric flux tubes behave strongly dynamic as predicted from numerical simulations (see Tab. 1). The formation of kG flux tubes by convective collapse would be accompanied by strong down drafts. In this statistical approach each signal represents a certain state of flux tube evolution. The remaining downflow found on average over all individual measurements could therefore mean that a significant part of measured features are in the process of formation. Also the downdraft surrounding a flux tube could lead to a redshift of the resulting V profile if these flows partially penetrate into the outer flux tube areas leading to a downstream magnetopause. This might also be an explanation for the dependence of the measured downflows with the fill-fraction: assuming the downflow is only located in a thin magnetopause whereas the gas in the interior of the flux tube is almost at rest. Then the contribution from the downstreaming parts to the V profile averaged over the whole flux tube would be much larger in case of a small flux tube (small fill fraction) than for larger magnetic elements. Another possibility to explain the much smaller flows found for large fill fraction might be that in this case the measurement is averaged over several individual flux tubes, so that tubes in the state of upflows cancel partially the downflows in other tubes. Or, a field with a higher fill fraction like what is present in the active region might suppress convective motions on a larger scale leading to generally suppressed dynamics. In any case the spatial resolution is still not sufficient to give an unambiguous answer on exactly how the flows and asymmetries are formed. Our results compare well with similar but independent measurements obtained with the ZIMPOL I polarimeter (Grossmann-Doerth et al. 1996). On the other side spatially and temporally integrated Stokes-V measurements with the FTS instrument (Solanki & Pahlke 1988) show much smaller Doppler shifts. The spatial integration leads to a selection effect toward larger magnetic features revealing higher V amplitudes. E.g. a highly redshifted V signal of small amplitude contributes much less to the resulting V profile of a spatially averaged measurement than the less shifted, large V signals. Figure 9 shows a spatially and temporal averaged V spectra for the magnetic network from our measurements. The resulting small downdraft compares well with the FTS results.

3 Formation of magnetic elements

Referring to numerical simulations, the formation of flux tubes as well as the interaction of magnetic elements with the granulation should lead to significant changes in the Doppler shift and shape of resulting V profiles on times scales of a few seconds to minutes (Steiner et al. 1998, Grossmann-Doerth et al. 1998). In order to obtain a better temporal resolution only small scans with the spectrograph can be performed. This of course limits the covered area on the sun. Figure 10 shows the example of a 20 min times series of a

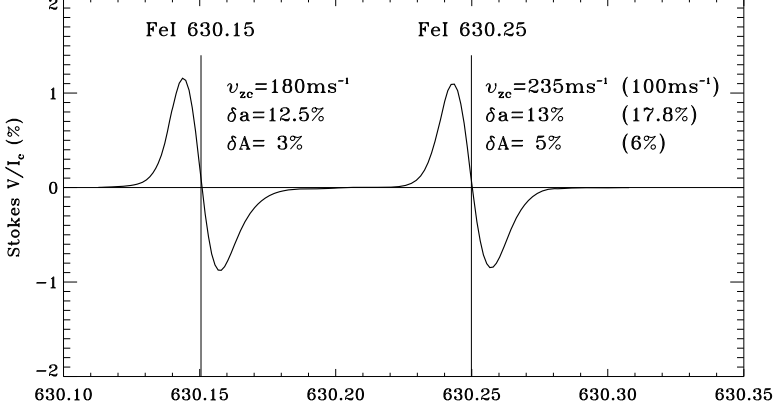

Figure 9: Spatially and temporally integrated ASP V spectra. The profile is averaged over a 10 arcsec^2 area in the network and over 3 consecutive scans (Δt = 51 min). The values for Doppler velocity and asymmetry are shown and compared with results from FTS observations (parenthetical).

quiet sun region. The series consists of 20 small scans of 10 steps each. The Doppler velocities obtained from Stokes-I reveal the photospheric 5 minute oscillations. From Stokes-V the temporal evolution of the magnetic features can be investigated.

3.1 Indications for convective collapse

Two examples for the formation of magnetic elements are shown in Fig. 11. Further explanations on the plots are given in the subtitles. In both cases the formation of the magnetic elements (negative polarity, black scaled) occurs during the second half of the sequence. In the first half no or only very weak and distributed magnetic flux is visible which finally starts to become spatially more and more concentrated while the V amplitude increases. During this *formation process* the downflow within the magnetic field increases dramatically while the amplitude asymmetry starts to decrease. The formation occurs at the outer granular boundary and in the intergranular region. The values for the V amplitude, the velocity and asymmetry for the magnetic elements and the Doppler velocity from Stokes-I at the location of the elements are shown in Fig. 12. This behavior compares very well with what we would expect from the convective collapse. The weak V profiles do not allow obtainment of precise values for the fieldstrength. Better SNR i. e. longer integration time or measurements in the infrared of such events can help to finally identify the formation of kG flux tubes by convective collapse. Recently Khomenko et al. (1999) observed the amplification of the magnetic field strength from below 300 G to about 500 G for a magnetic feature in the quiet sun by using the Tenerife Infrared Polarimeter (TIP, Martínez Pillet et al. 1999). The ampli-

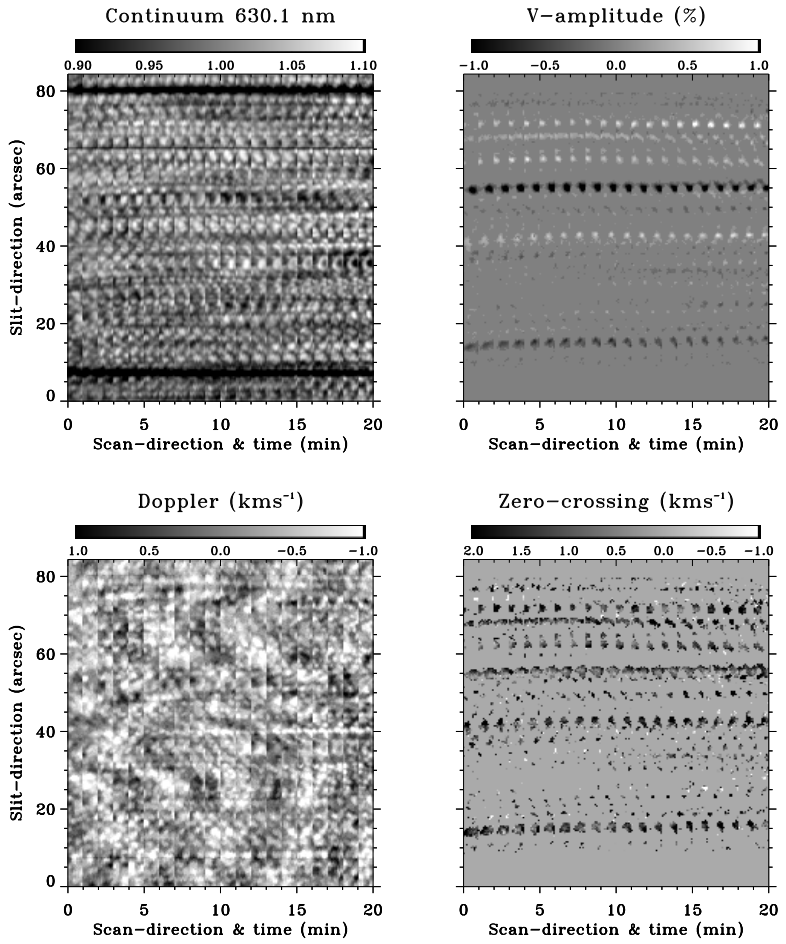

Figure 10: Spatial maps of a time series for a quiet sun region at disc center. Each map consist of 20 consecutive spatial scans over a region of 3.75×74 arcsec^2. The upper row shows the continuum sprectroheliograms at 630.1 nm and the map for the Stokes-V amplitude. In the second row the Doppler velocity from Stokes-I line core shifts and the Stokes-V zero-crossing velocity are shown. All information was obtained from FeI 630.25 nm. The bars on top of the plots denote the plot scaling.

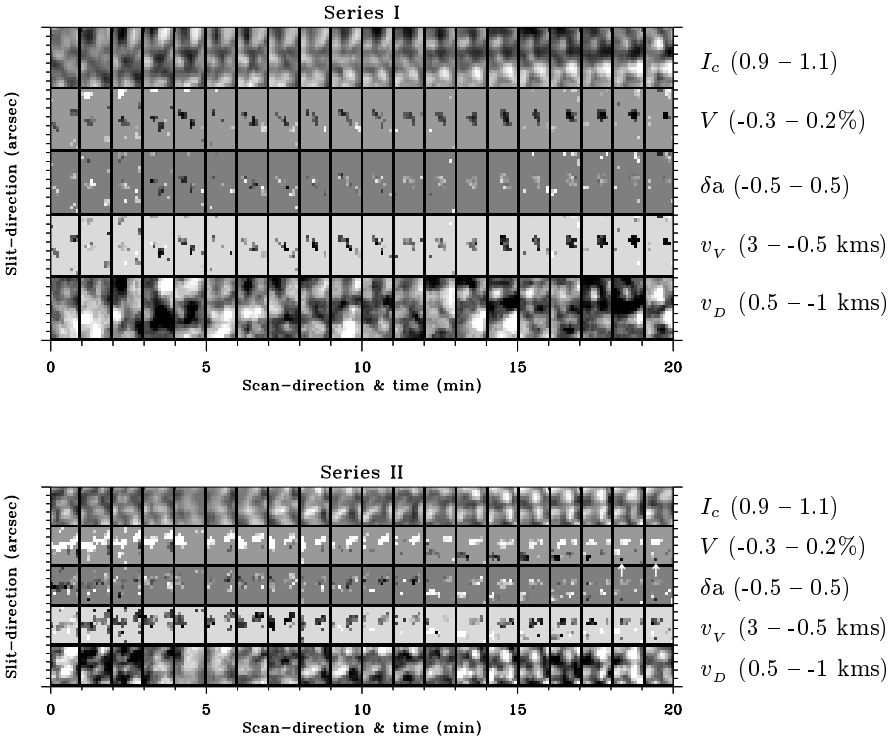

Figure 11: Formation and concentration of magnetic elements. The figures show details of time series like the one shown in Fig. 11. The first row consists of 20 consecutive spetroheliograms in the continuum. The second row shows the Stokes-V amplitude, with negative polarity dark scaled. In the third row the amplitude asymmetry is displayed followed by the velocity in the magnetic field (dark – downflow/bright – upflow). The last row shows the Doppler velocity from Stokes-I. The tickmarks along the slit direction correspond to 1 arcsec (in both directions). The scaling of the plots is given on the right side of each single row. In both examples a magnetic element of negative polarity is formed. The formation starts in both cases after minute 10. In series II the V signals finally occurs from only one pixel marked by white arrows.

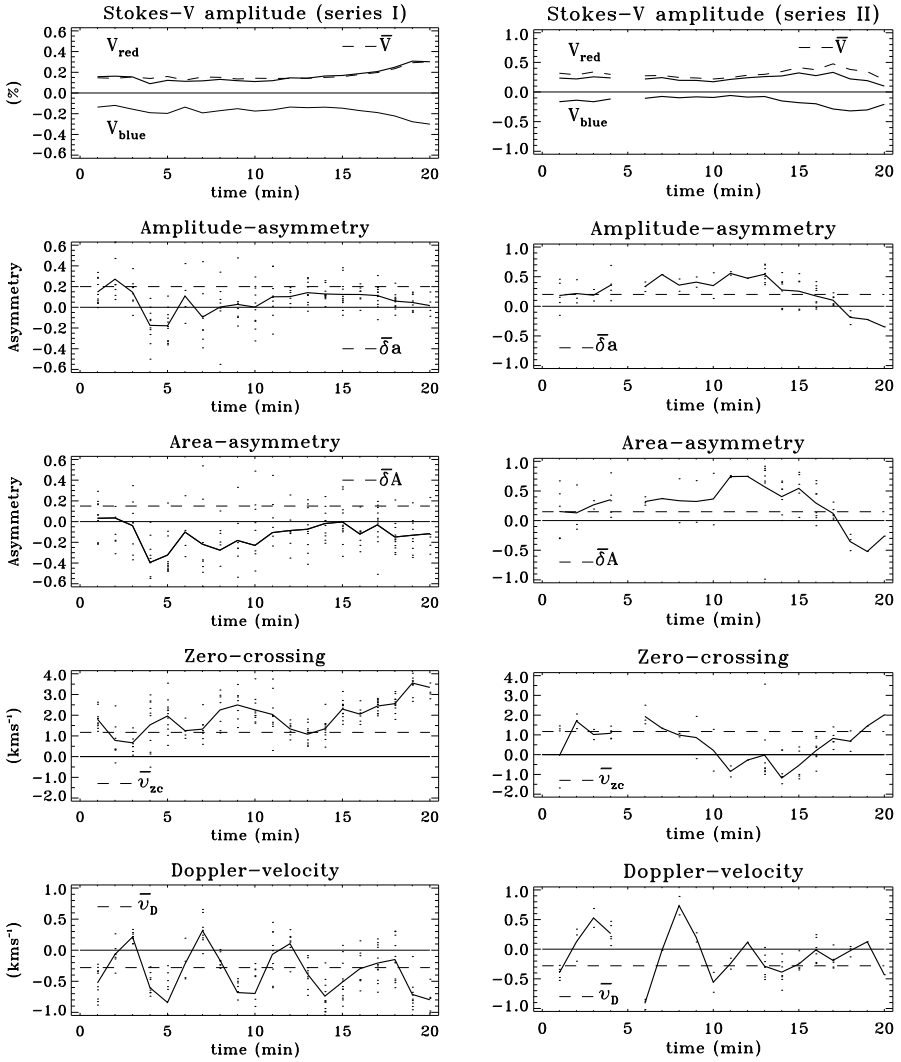

Figure 12: Temporal development of Stokes-V parameters and the Doppler-velocity during the formation and concentration of magnetic elements. The solid lines denote the mean value over the investigated magnetic element within each scan, the dots represent the value for each data point with a significant V signal. The horizontal dashed lines denote the mean-value over all Stokes-V profiles of the observation. The negative mean Doppler velocity (blue-shifted/upflow) is due to the *convective blueshift* of the mean I profile. The left column shows the values for the example of series I, the right for series II. See also Fig. 11.

fication was also accompanied by an increasing downflow of up to 3 kms^{-1}, followed by an upward propagating shock wave which seems to lead to the destruction of the magnetic feature.

4 Rising flux tubes in a young active region

Young, evolving active regions provide the opportunity to prove and develop fundamental models on the origin and formation of bipolar active regions. The basic idea is, that the magnetic flux from which active regions are built up originate from the bottom of the convective zone where the magnetic field is thought to be generated and stored. From there flux tubes rise buoyantly through the convection zone and finally enter into the photosphere where an active region is formed. Evidence that sunspots of a bipolar group are footpoints of a flux-tube loop (or bundle of flux tubes) are found from Hα and corona images, where loops are visible connecting the preceding and following spot(s) (e. g. Bruzek 1967). In an early state of formation, the preceding and following[2] spots separate from each other while along the neutral line between the bipolar region new magnetic flux emerges (Zwaan 1985 und 1992, Strous 1996). This is consistent with the image that a major part of the flux tube already entered higher atmospheric layers and formed an omega-shaped loop system that reaches into the corona while fragmented parts of the original flux tube are still rising through the photosphere. The flux tubes forming the active region can bear imprints from their earlier history, i. e. the process of leaving the magnetic belt at the bottom of the convection zone, the rise through the convection zone, and the interaction with convective motions in the deep photosphere. Simulations of such rising flux tubes are able to reproduce the distinct tilt of bipolar active regions with respect to the equator. They also predict a larger field inclination in the following compared to the preceding spot (Caligari et al. 1995). Simulations also predict longitudinal flows along flux tubes arising from a combination of effects, namely, sliding motion associated with the Parker instability, Coriolis forces, and remnants of a longitudinal flow in the original equilibrium of the flux tube (for review see Moreno-Insertis 1997).

Similar to the small scale kG flux tubes there must be an efficient mechanism to amplify the field strength up to several kG. The buoyantly rising flux tube expands (and maybe fragments partially) when entering the photosphere so that the field strength drops to the equipartition field strength of approx. 50 mT.

4.1 Observations

The obtained data of a young active region provides a good opportunity to investigate several aspects of the formation process of active regions. The high resolution of about 0.8 arcsec allows investigation of small scale effects.

[2]With respect to the solar rotation from east to west.

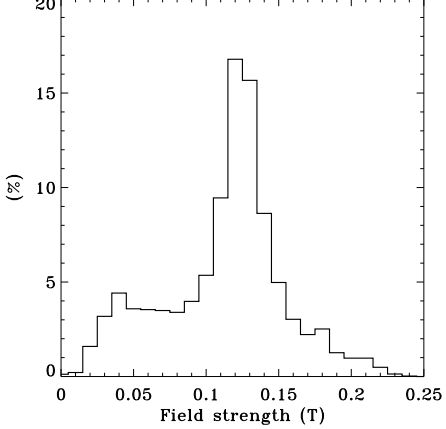

Figure 13: Distribution of the magnetic field strength in a young active region.

Because all 4 Stokes parameter are available, the whole vector of the magnetic field (field strength B, inclination γ and azimuth α) can be derived from the inversion of the measured Stokes vector (Skumanich & Lites 1987). The location of the region close to disc center allows to distinguish between horizontal and vertical motions. Examples of the data are shown in Figs. 6 and 7. Further informations can be found in Sigwarth et al. 1998 and Sigwarth et al. 1999a.

4.2 Signatures of emerging flux

The active region NOAA 7968 was first reported two days prior to our observation (Solar-Geophysical Data 1996). The observation covers about 70 min during which the measurable magnetic flux increases from $4 \cdot 10^{13}$ Wb to $4.5 \cdot 10^{13}$ Wb which indicates the ongoing flux emergence[3]. The following and preceding spot are separating from each other with a relative velocity of 440 ms^{-1}.

The histogram for the field strength (Fig. 13) for all data points with a total polarization $P = \sqrt{(Q^2 + U^2 + V^2)}/I_c \geq 0.4\,\%$ shows two distinct components: A strong field component, originating from plage and spots and a weak field component with field strength around 40 mT. The weak fields are found around the preceding spot where a penumbra starts to develop and along the neutral lines between the spots. Both locations are also associated with strongly inclined fields. In Fig. 14 the inclination is plotted against the field strength. It is obvious that the weak field component is associated with strongly inclined fields whereas strong fields are almost vertical. Parts of the horizontal fields are associated with an upflow of up to 1 kms^{-1} as can be seen in Fig. 14 where the inclination is plotted versus the line of sight

[3]Flux is only counted for the polarity of the preceding spot because parts of the following spot were moving out of the field of view during the observation.

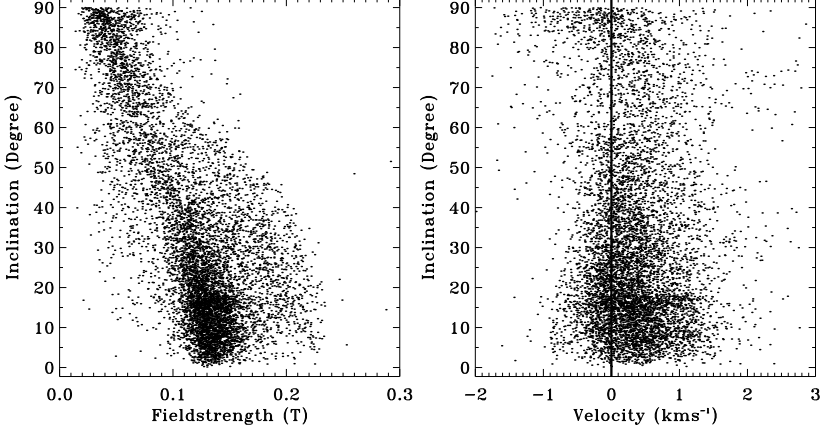

Figure 14: Inclination of the magnetic field in an emerging flux region plotted versus the field strength (left) and the vertical velocity in the magnetic field (right).

velocity. The velocity is obtained from the Doppler shift of Stokes-V profiles and represents gas motion within magnetic fields only. These upmoving fields are located in small patches along the neutral line. The correlation found between the inclined fields, field strength and vertical flows is in agreement with measurements of Lites et al. (1998) for several emerging flux regions.

A possible explanation is, that the weak, horizontal fields along the neutral line represent the top of rising flux tubes with equipartition fieldstrenth. Very rapidly the fieldstrength seems to increase whereas the fieldlines become mostly vertical. The gas captured within the rising flux tubes leads to the observed blueshift of the V spectra.

4.3 Upwelling in a young sunspot

In the central part of the preceding spot an upflow exceeding 0.5 kms^{-1} is present. Figure 15 shows the line of sight velocity within magnetic fields plotted against the field strength separated for the positive polarities (including the preceding spot) and negative polarities (including the following spot). While most data points reveal a downflow, (positive velocities) for a small location within the preceding spot (field strength $>$ 0.2 T), upflows between 0.5 and 1 kms^{-1} are present (data points marked with crosses). On the other side in the following spot a weak downflow is present (data points originating from the f-spot are also marked by crosses). The enhanced areas within the spots shown in Fig. 16 mark the locations where the flows are observed.

The calibration of the velocities derived from shifts of the V profiles has an accuracy of $\pm$ 220 ms^{-1} (systematic and statistical error). The measured line-of-sight velocities in the spot are probably affected by the ongoing separation of the polarities. If the relative horizontal velocity between f- and p-spot is fully attributed to the p-spot this would lead to a line-of-sight velocity

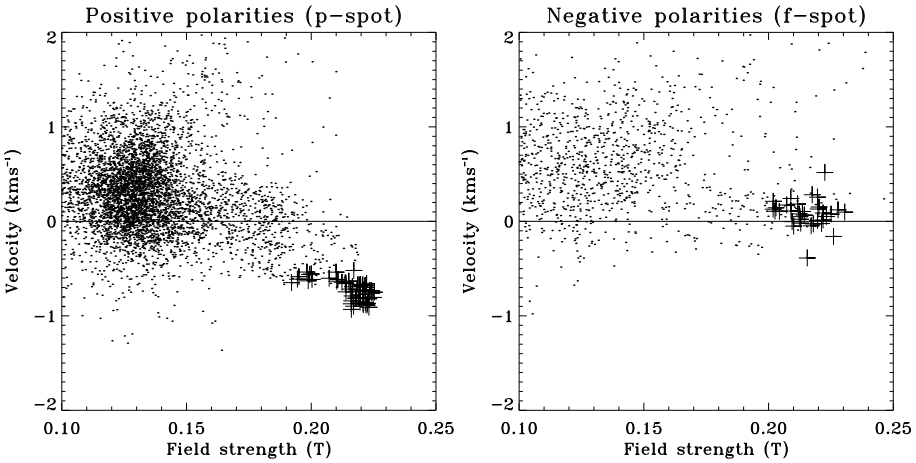

Figure 15: Plots of the vertical flows in a young active region vs. the magnetic field strength. The two magnetic polarities are considered separately in left and right panel. Negative velocities correspond to an upflow. The points marked with crosses are located in the darkest regions within the spots (see also Fig. 16).

(upflow) of ≈ 100 ms^{-1}. Even in this case the measured upflow in the p-spot would remain significant.

In general systematic photospheric flows in the umbrae of mature sunspots are insignificant (Beckers 1977, Schmidt & Balthasar 1994). Evershed flow and siphon flow can also be ruled out as cause of the measured upflow (Sigwarth et al. 1998). A possibility that is in accordance with the observed velocities is the counterflow against the direction of rotation (in a rotating frame of reference), which is caused by angular momentum conservation of the plasma carried by a rising magnetic flux loop. Such flows have been found in numerical simulations of flux tubes rising in the convection zone (Moreno-Insertis et al. 1994, Caligari et al. 1995, Fan et al. 1994). At the solar surface, the counterflow would correspond to upflows in the preceding spots and downflows in follower spots. A detailed comparison between the models and the observations cannot be made since the simulations do not cover the actual flux emergence at the surface and the later evolution of the sunspots. Nevertheless, the flow direction (upflow in the p-part and downflow in the f-part) and also the magnitude of the upflow velocity are in agreement with the results of simulations that best reproduce other observed properties of sunspot groups like emergence latitudes, tilt angles, and geometrical asymmetry (Moreno-Insertis 1997).

The evolutionary phase caught by the observations appears to provide the best opportunity to detect a possible surface manifestation of such a flow: (a) in the early phases of flux emergence the rapid ascent of the apex and the sliding motions associated with the fast rise of a fragmented flux loop in a strongly stratified background probably dominate, while (b) at later times (in mature sunspots) hydrostatic equilibrium along the field lines has established

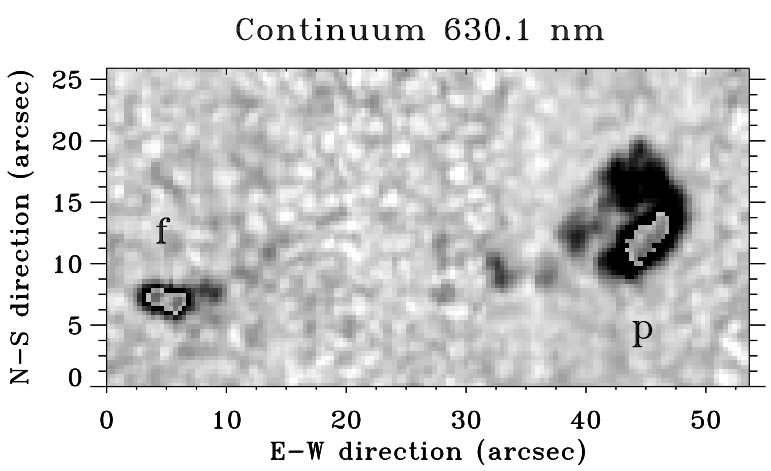

Figure 16: Continuum spectroheliogram of an emerging flux region. The preceding (p) spot is on the right (west) side, the following (f) spot on the left. The enhanced areas within the spots mark the location where the flows are observed. Disc center is in the direction of the lower right corner.

itself. Note that the longitudinal counterflow cannot be maintained for a long time after the emergence as a stationary since the loop is then connected through the very tenuous coronal layers, through which the large mass flux of the flow cannot be driven. Therefore, the flows in the p- and in the f-spot become unrelated to each other and it is conceivable that the f-spot is already nearly hydrostatic while the upflow in p-spot still continues.

So far this measurement of an upwelling in a sunspot has been the only one. The same active region was investigated by Chapman (1998) 7 h later where he did not find upflowing material between p-spot and f-spot nor did he find a significant upflow within the spots. The observations were performed in the same spectral line than we used but suffer from very low spatial resolution. Also the velocities were measured from Stokes-I only so it is not possible to distinguish between flows of magnetic and non-magnetic gas. Therefore upflows along the neutral line which we found to occur on spatial scales below 2 arcsec cannot be detected by low resolution Stokes-I measurements. The upflow in the p-spot might be decreased by the time of this measurement. But even if the upflow was still present it is questionable whether it could be detected at such low spatial resolution which is of the same order than the upflowing area within the spot.

More observations of young sunspots, preferably located at or very near disc center, are needed in order to examine whether the flow pattern found in this particular case is a general feature.

5 Future perspectives

The operation of adaptive optics with existing telescopes will allow performance of longer integration times and longer time series of spectropolartimetric measurements with spatial resolution of 0.5 to 1 arcsec^2. Figure 17 shows the first measurements of the full Stokes vector of G-band bright points (magnetic elements) in the quiet sun by using the ASP and the NSO low order adaptive optic system (Rimmele et al. 1999). Although the integration time is doubled compared to the observations presented in this paper, a spatial resolution of 1 arcsec was achieved. The high signal to noise ratio allows the measurement of circular polarization of 0.1 % V/I_c. Also the size of the bright point (FWHM) is only 0.25 arcsec magnetic field can be found in an area of about 2 arcsec around it with maximum flux density at the location of the bright point. Observations like this will help to improve our understanding of the nature of flux concentration in the photosphere but we are still unable to spatially resolve the smallest magnetic structures.

The results of the presented investigation as well as the results from numerical simulations indicate that observations with higher spatial resolution are needed in order to solve ambiguities arising from observations with 0.5 arcsec to 1 arcsec spatial resolution. To be able to compare observations with models quantitatively in order to understand in detail the physical processes leading e. g. to the observed asymmetry of Stokes-V profiles or to the observed flows in flux tubes, a consistent resolution of 0.1 arcsec or better will be necessary. Also a larger photon flux will be essential in order to be able to perform spectropolarimetry with sufficient signal to noise ratio at such high spatial resolution. Current solar high resolution facilities with typical 0.45 m to 0.8 m aperture cannot provide this requirement. Therefore the need of large aperture solar telescopes is evident. Currently strong efforts are being made in order to get a new generation of larger aperture solar telescopes into operation. The upgraded New Swedish Solar Telescope (NSST) with an aperture of 0.97 m is scheduled to go into operation in 2001. The German solar community is planning to replace an existing 0.45 m Vacuum Gregory Coudé Telescope at the Observatory del Teide, Tenerife, with the open 1.5 m telescope GREGOR. In the US an Advanced Solar Telescope (AST) with an aperture of 3 m to 4 m is currently proposed and planned to bring into operation by the end of the next decade.

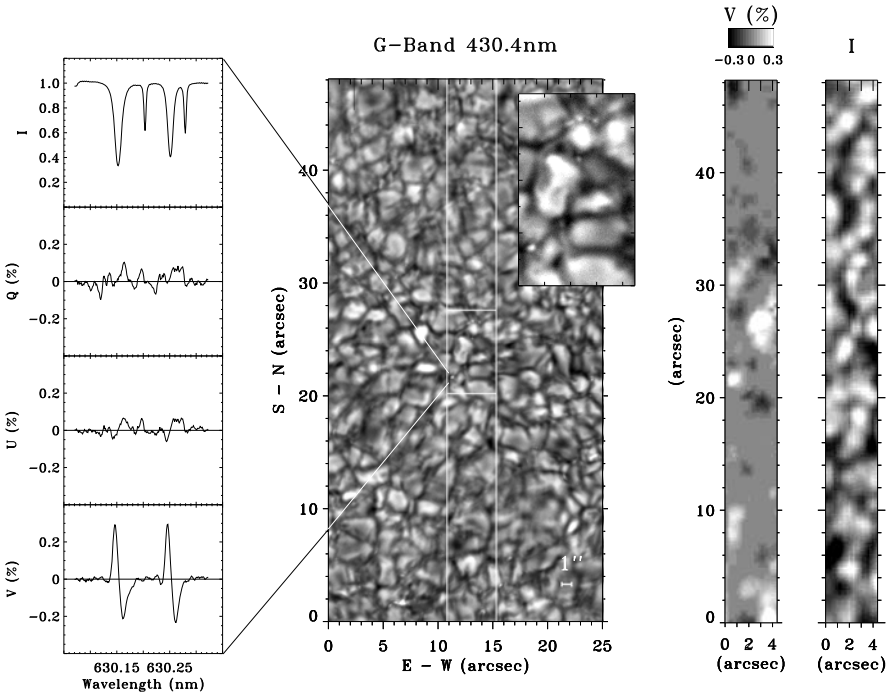

Figure 17: Stokes vector polarimetry of G-band bright points with adaptive optics. Simultaneously to the Stokes spectra images in the G-Band where obtained. The vertical white lines in the G-band image mark the scanning range of the spectrograph. In the enlarged frame (area marked by the white box) several bright points are visible. On the right side the V amplitude and continuum map from the ASP scan are shown. The pixel scale for the G-band image is 0.047 arcsec^2/pixel, for the ASP 0.37×0.4 arcsec^2/pixel. The integration time for the G-band was 10 ms, for the spectra 4.2 sec. The left column show the Stokes spectra for a G-band bright point.

Acknowledgements: The results presented in this paper were obtained during my PhD work at the Kiepenheuer-Institut für Sonnenphysik (KIS), Freiburg, Germany. I would like to thank Wolfgang Schmidt (KIS) and Michael Knölker (HAO) for their support and collaboration in this work and many other colleagues from the KIS for numerous helpful discussions. The observations where done at the National Solar Observatory/Sacramento Peak where I obtained encouraging help from K. S. Balasubramaniam and the whole NSO/SP staff. I would also like to acknowledge the support from the ASP group at the High Altitude Observatory (HAO), Boulder. This work is supported by the visitor program at HAO/NCAR, the EOARD-WOS service and by the Deutsche Forschungsgemeinschaft under grant Schm 1168/1–2.

References

Auer, L. H., Heasley, J. N., 1978, A&A 64, 67

Beckers, J. M., 1977, ApJ 213, 900

Berger, T. E., Title, A. M., 1996, ApJ 463, 365

Bruzek, A., 1967, Sol. Phys. 2, 451

Caligari, P., Moreno-Insertis, F., Schüssler, M., 1995, ApJ 441, 886

Cattaneo, F., 1999, ApJ 515, L39

Chapman, G. A., 1998, Sol. Phys. 183, 15

Dravins, D., Lindgren, L., Nordlund, Å., 1981, A&A 96, 345

Elmore, D. F., Lites, B. W., Tomczyk, S., et al., 1992, Proc. SPIE 1746, 22

Fan, Y., Fisher, G. H., McClymont, A. N., 1994, ApJ 436, 907

Frazier, E. N., Stenflo, J. O., 1972, Sol. Phys. 27, 330

Galloway, D. J., Weiss, N. O., 1981, ApJ 243, 945

Giovanelli, R. G., Ramsay, J. V., 1971, in: *Solar Magnetic Fields*, R. Howard (ed.), Reidel, Dordrecht, IAU Symp. 43, p. 293

Grossmann-Doerth, U., Schüssler, M., Solanki, S. K., 1988, A&A 206, L37

Grossmann-Doerth, U., Schüssler, M., Solanki, S. K., 1989, A&A 221, 338

Grossmann-Doerth, U., Keller, C. U., Schüssler, M., 1996, A&A 315, 610

Grossmann-Doerth, U., Schüssler, M., Steiner, O., 1998, A&A 337, 928

Grossmann-Doerth, U., Schüssler, M., Sigwarth, M., Steiner, O., 1999, A&A (submitted)

Howard, R., Stenflo, J. O., 1972, Sol. Phys. 22, 402

Illing, R. M. E., Landmann, D. A., Mickey, D. L., 1974, A&A 35, 327

Illing, R. M. E., Landmann, D. A., Mickey, D. L., 1975, A&A 41, 183

Keller, C. U., 1992, Nat 359, 307

Khomenko, E., Collados, M., Bellot, Rubio L. R., et al., 1999, in: *Proc. of the 9th European Meeting on Solar Physics, Florence*, ESA (in press)

Lin, H., 1995, ApJ 446, 421

Lites, B. W., Skumanich, A., Martínez Pillet, V., 1998, A&A 333, 1053

Martínez Pillet, V., Lites, B. W., Skumanich, A., 1997, ApJ 474, 810

Martínez Pillet, V., Collados, V., Sánchez Almeida, J., et al., 1999, in: *High resolution solar physics: Theory, observations, and techniques*, T. Rimmele, K. S. Balasubramaniam, R. Radick (Eds.), ASP Conference Series, Vol. 183, p 264

Moreno-Insertis, F., 1997, in: *The Inconstant Sun*, eds. G. Cauzzi, C. Marmolino, Memorie Soc. Astron. Ital., Vol. 68, p. 429

Moreno-Insertis, F., Caligari, P., Schüssler, M., 1994, Sol. Phys. 153, 449

Parker, E. N., 1963, ApJ 138, 552

Parker, E. N., 1978, ApJ 221, 368

Povel, H. H., et al., 1991, Proc. SPIE, 1542, 186

Rimmele, T. R., Dunn, R. B., Richards, K., Radick, R. R., 1999, in: *High resolution solar physics: Theory, observations, and techniques*, T. Rimmele, K. S. Balasubramaniam, R. Radick (Eds.), ASP Conference Series, Vol. 183, p 222

Schmidt, W., Balthasar, H., 1994, A&A, 283, 241

Schüssler, M., 1996, in: *Solar and astrophysical magnetohydrodynamic flows*, K. C. Tsinganos (Ed.), ASI Series 481, p. 17

Sigwarth, M., 1999, Dissertation , Universität Freiburg

Sigwarth, M., Schmidt, W., Schüssler, M., 1998, A&A 339, L53

Sigwarth, M., Balasubramaniam, K. S., Knölker, M., Schmidt, W., 1999a, A&A 349, 941

Sigwarth, M., Balasubramaniam, K. S., Knölker, M., 1999b, in: *High resolution solar physics: Theory, observations, and techniques*, T. Rimmele, K. S. Balasubramaniam, R. Radick (Eds.), ASP Conference Series Vol. 183, p. 36

Skumanich, A., Lites B. W., 1987, ApJ 322, 473

Solanki, S. K., 1986, A&A 168, 311

Solanki, S. K., 1993, Space Science Review 63, 1

Solanki, S. K., Stenflo, J. O, 1984, A&A 140, 185

Solanki, S. K., Stenflo, J. O, 1985, A&A 148, 123

Solanki, S. K., Pahlke, K. D., 1988, A&A 201, 143

Solar-Geophysical Data prompt reports, 1996, H. E. Coffey (Ed.), Vol. 624, p. 42–45

Spruit, H. C., Zweibel, E. G., 1979, Sol. Phys. 62, 15

Steiner, O., 1999, in: *High resolution solar physics: Theory, observations, and techniques*, T. Rimmele, K. S. Balasubramaniam, R. Radick (Eds.), ASP Conference Series Vol. 183, p. 15

Steiner, O., Grossmann-Doerth, U., Knölker, M., et al., 1998, ApJ 495, 468

Stenflo, J. O., 1973, Sol. Phys. 32, 41

Stenflo, J. O., Harvey J. W., 1985, Sol. Phys. 95, 99

Stenflo, J. O., Harvey, J. W., Brault, J. W. et al., 1984, A&A 131, 333

Stenflo, J. O., Solanki, S. K., Harvey, J. W., 1987, A&A 171, 305

Stenflo, J. O., Keller, C. U., Gangdorfer, A., 1998, A&A 329, 319

Strous, L. H., 1996, ApJ 306, 947

Weiss, N. O., 1966, Proc. Roy. Astron. Soc. A, 293, 310

Weiss, N. O., 1994, in: *Lectures on solar and stellar dynamos*, M. R. E. Proctor, A. D. Gilbert (Eds.), Cambridge Univ. Press, p. 59

Wiehr, E., 1985, A&A 149, 217

Zwaan, C., 1985, Sol. Phys. 100, 397

Zwaan, C., 1992, in: *Sunspots, Theory and observation*, J. H. Thomas, N. O. Weiss (Eds.), ASI Series 375, p. 75